

Universal Theory of Dynamic Force Microscopy for Exact and Robust Force Reconstruction Using Multiharmonic Signal Analysis

Sunghoon Kim[✉], Joon-Hyuk Ko[✉], and Wonho Jhe^{✉*}

Center for 0D Nanofluidics, Institute of Applied Physics, Department of Physics and Astronomy, Seoul National University, Seoul 08826, Republic of Korea

 (Received 7 October 2020; revised 27 December 2020; accepted 22 January 2021; published 19 February 2021)

Force reconstruction in dynamic force microscopy (DFM) is a nontrivial problem that requires the deconvolution of integrals. However, conventional reconstruction methods, which recover forces from single-frequency motion of the cantilever at its resonance, exhibit non-negligible error and reconstruction instability in the highly nonlinear force regime when the tip oscillates with its amplitude comparable to the decay length of the interaction. Here, we develop a theoretical platform of DFM based on multiharmonic signal analysis for exact and robust reconstruction of conservative and dissipative forces, valid for all oscillation amplitudes and entire tip-sample distances in both amplitude- and frequency-modulation atomic force microscopy. We achieve accuracy improvement by an order of magnitude for oscillation amplitudes comparable to or larger than the decay length, and by 2 orders of magnitude for smaller amplitudes at the force minimum, even in cases where conventional methods show poor accuracy ($\gtrsim 5\%$). Moreover, we obtain greater robustness with respect to the oscillation amplitude error, resulting in a fivefold increase in reconstruction precision. Our results demonstrate a fast and versatile reconstruction scheme for nano-mechanical force characterization, with higher harmonics measured with sufficient signal-to-noise ratio, which provides unprecedented accuracy and stability beyond conventional methods.

DOI: [10.1103/PhysRevLett.126.076804](https://doi.org/10.1103/PhysRevLett.126.076804)

Introduction.—The invention of atomic force microscopy (AFM) [1] has opened the doors to quantitative characterization of the structures and forces at the molecular and atomic level [2–4]. The high resolution is achieved by using a sharp probe tip attached at the end of the cantilever, whose deflection is monitored during its gradual approach to the surface. The need for a higher signal-to-noise ratio (SNR) and greater sensitivity to the short-range forces has led to the introduction of dynamic force microscopy (DFM) where the oscillating motion of the AFM probe is detected as it is driven externally. Employing AFM in the dynamic mode, however, requires the calculation of the interaction forces from the acquired experimental data depending on the operating scheme: amplitude-modulation AFM (AM-AFM) [5] or frequency-modulation AFM (FM-AFM) [6].

Force reconstruction in DFM is a nontrivial problem since it involves the inversion of integrals. Previous works proposed the use of iterative calculations [7,8], matrix inversions [9], infinite summations of higher order derivatives [10], and Chebyshev polynomials [11]. Yet, such methods suffer from limited practicality and/or underperformance because they generally require heavy calculations to achieve good accuracy [12,13]. In practice, the integration method of Sader and Jarvis [14], called the Sader-Jarvis (SJ) method, has been most widely used in both FM-AFM [14] and AM-AFM [12,15] operations, since it provides good approximation to the underlying forces using simple integrals.

Regardless of its wide usage, however, the SJ method has recently been reported to yield a non-negligible error and exhibit reconstruction instability when the oscillation amplitude is comparable to the decay length, λ , of the interaction forces [12,14,16–18]. A strategy to “bypass” this problem would be to use amplitudes smaller or larger than λ despite the requirement of additional experimental procedures to identify (possibly multiple) λ 's [18,19], which are generally not known *a priori*. However, there is a trade-off: since such a bypass strategy sacrifices both the SNR [20] and the sensitivity to the short-range forces [6], one requires not only costly instruments and long data acquisition times to achieve low noise, but also excessive experimental procedures to isolate the short-range contributions from the measured forces. Indeed, to optimize the signal measurement, amplitudes comparable to λ have been used in numerous experiments, particularly in recent research in condensed-matter physics [21–25]. Nonetheless, when such amplitudes are used, conventional force-reconstruction procedures fail to accurately recover the force in a reliable manner. This is due to the discrepancy between the assumption used in the reconstruction formulas (i.e., single-frequency cantilever motion at resonance) and the actual cantilever dynamics which can become significantly anharmonic, especially in the rapidly changing regime of the force. Therefore, one still needs an accurate and robust force reconstruction platform for DFM, valid in the entire range of amplitudes.

In multiharmonic AFM (MHAFM), the anharmonicity of the cantilever motion is used to enhance the capability of the conventional DFM. The higher harmonic signals are simultaneously detected in AM-AFM or FM-AFM operations to attain greater spatial resolutions [26–29] and characterize the local properties in more detail [30–33]. Several works used additional modulation techniques to extract nonlinear dependence of the tip-sample interactions [34–36]. While understanding higher harmonic motions in DFM is crucial for overcoming the “pothole” in conventional force reconstructions, theoretical formulations of MHAFM remain incomplete; existing analytical expressions for higher harmonic signals of arbitrary harmonic order are derived only for high-vacuum FM-AFM operations [37], still requiring a general framework for both MHAFM modes to resolve the “pothole.”

In this Letter, we develop a versatile MHAFM platform for exact, robust, and efficient force reconstruction. First, we provide analytical formulas for higher harmonic responses in DFM, which we then invert to derive explicit reconstruction formulas for conservative and dissipative forces, valid for all oscillation amplitudes and the entire tip-sample distances. Analytic expressions of these formulas are derived separately for each operation mode of DFM. We demonstrate the exactness of our formulas by performing force reconstruction for the Lennard-Jones–type force model, and find that our approximate reconstruction results, obtained by including only a finite number of harmonics, show superior accuracy over the SJ method. Finally, the robustness of our MHAFM force reconstruction scheme against the oscillation amplitude error is demonstrated using the Stillinger-Weber–type force model, which clearly shows that our approach remarkably overcomes the force inversion instability inherent in the conventional methods.

The motion of the cantilever probe in DFM is typically modeled as a driven harmonic oscillator in the presence of tip-sample interaction [10,14],

$$m\ddot{\xi} + b\dot{\xi} + k\xi = kA_d \cos \omega t + F_{\text{int}}, \quad (1)$$

where ξ is the relative position of the probe with respect to the equilibrium position, m the effective mass, b the damping coefficient, and k the stiffness of the probe. The coefficients on the left-hand side of the equation are related to the unperturbed resonance frequency ω_0 and the quality factor Q , where $b = m\omega_0/Q$ and $k = m\omega_0^2$. The right-hand side of the equation represents the tip-sample interaction force F_{int} and the external driving force with driving amplitude A_d and frequency ω . As the cantilever approaches the surface and F_{int} becomes noticeable, the nonlinearity of F_{int} within the oscillation range leads to the multiharmonic motion of the probe. Thus, ξ can be described in terms of the relative distance z between the tip and substrate atoms;

$$\xi(z, t) = \xi_0(z) + \sum_{n=1}^{\infty} A_n(z) \sin [n\omega t + \theta_n(z)], \quad (2)$$

where $A_n(z)$ and $\theta_n(z)$ denote the amplitude and phase, respectively, of the n th harmonic motion and $\xi_0(z)$ is the mean deflection of the probe.

The interaction force can be decomposed into the conservative and dissipative (nonconservative) terms,

$$F_{\text{int}}(z, \dot{z}) = F_c(z) + F_{\text{nc}}(z, \dot{z}). \quad (3)$$

Combining Eqs. (1) and (3), we obtain the dissipation energy of the probe for a single oscillation,

$$\begin{aligned} -\Delta E &= \int_0^T dt \dot{\xi} F_{\text{nc}} \\ &= \int_0^T dt \dot{\xi} (m\ddot{\xi} + b\dot{\xi} + k\xi - kA_d \cos \omega t - F_c), \end{aligned} \quad (4)$$

which can be rewritten in terms of multiharmonic signals as, using Eq. (2),

$$\Delta E = \pi k \left(A_d A_1 \cos \theta_1 - \frac{\omega}{Q\omega_0} \sum_{n=1}^{\infty} n^2 A_n^2 \right). \quad (5)$$

Note that the dissipation energy is fully expressed by the multiharmonic responses, with no dependence on the explicit form of F_{nc} . Moreover, it consists of the external energy influx from the drive (the positive term) and the internal dissipation energy (the negative terms), where the higher harmonic terms ($n > 1$) reflect the additional internal dissipation due to the higher harmonic motions. Indeed, the single amplitude approximation of Eq. (5) reduces well to the previously reported results [6,10,38].

Now, we consider F_{nc} having explicit velocity dependence of the form,

$$F_{\text{int}}(z, \dot{z}) = F_c(z) - \Gamma(z)\dot{z}, \quad (6)$$

where $\Gamma(z)$ is the friction coefficient [37]. This particular form is chosen for further investigation as it is one of the most conventional and intuitive representation of the dissipation force [10,12,37]. Inserting Eq. (6) to Eq. (1), we obtain the following equation of motion for the probe:

$$m\ddot{\xi} + b\dot{\xi} + k\xi = kA_d \cos \omega t + F_c(z + \xi) - \Gamma(z + \xi)\dot{\xi}. \quad (7)$$

From this equation, we proceed to derive explicit force reconstruction formulas, corresponding to the two MHAFM operation modes.

Amplitude-modulation MHAFM.—In amplitude-modulation MHAFM, the cantilever is driven at a constant driving amplitude and frequency, with the responses at both the driving frequency and its integer multiples being the experimentally measured quantities. To proceed, we assume $|A_1| \gg |A_n|$ for $n > 1$, corresponding to typical MHAFM experimental observations [27,28,33]. Also, we assume $z + \xi_0 \approx z$ in accordance with previous DFM

literature [4,10], as the mean deflection is negligible with the use of stiff cantilevers. Integrating Eq. (7) with the weight functions $\sin(n\omega t + n\theta_1)$ and $\cos(n\omega t + n\theta_1)$ gives,

$$\int_0^\pi \frac{d\tau}{\pi} F_c(z + A_1 \cos \tau) \cos n\tau = -\delta_{n1} \left(\frac{kA_d}{2} \sin \theta_1 \right) + \frac{1}{2} \text{Re}[\tilde{A}_n \tilde{H}_n^{-1}], \quad (8)$$

$$\int_0^\pi \frac{d\tau}{\pi} \Gamma(z + A_1 \cos \tau) \sin \tau \sin n\tau = \delta_{n1} \left(\frac{kA_d}{2A_1\omega} \cos \theta_1 \right) - \frac{1}{2A_1\omega} \text{Im}[\tilde{A}_n \tilde{H}_n^{-1}]. \quad (9)$$

Here, δ_{n1} is the Kronecker delta, $\tilde{A}_n \equiv A_n e^{i\theta_n}$ and $\tilde{H}_n \equiv H(i\omega) e^{in\theta_1} i^{1-n}$, where $H(i\omega) \equiv (k - m\omega^2 + i b\omega)^{-1}$ is the transfer function of the cantilever. Note that A_n and θ_n are uniquely determined by the above equations for any positive integer n .

Reconstruction of the force from the multiharmonic responses requires inversion of the integrals in Eqs. (8) and (9). Through several derivation steps (see Supplemental Material SM1 [39]), we derive the *exact* expressions for F_c and Γ using the multiharmonic signals,

$$F_c(z) = \int_z^\infty dz' \frac{kA_d}{A_1(z')} \sin \theta_1(z') + \sum_{m=1}^\infty \left\{ (-1)^m (2m-1) \times \int_z^\infty \frac{dz'}{A_1(z')} \text{Re}[\tilde{A}_{2m-1}(z') \tilde{H}_{2m-1}^{-1}(z')] \right\}, \quad (10)$$

$$\Gamma(z) = \frac{kA_d}{A_1(z)\omega} \cos \theta_1(z) + \sum_{m=1}^\infty \frac{(-1)^m}{A_1(z)\omega} \text{Im}[\tilde{A}_{2m-1}(z) \tilde{H}_{2m-1}^{-1}(z)]. \quad (11)$$

Frequency-modulation MHAFFM.—In FM-AFM, the driving amplitude and frequency are controlled to ensure fixed oscillation amplitude A_1 at the resonance frequency ω_{res} ($\theta_1 = 0$) by using feedback loops. Thus, frequency-modulation MHAFFM measures the resonance frequency shift $\Omega(z) \equiv [\omega_{\text{res}}(z) - \omega_0]/\omega_0$, driving amplitude $A_d(z)$, and higher harmonic responses $\tilde{A}_n \equiv A_n e^{i\theta_n}$. Using again the assumptions of $|A_1| \gg |A_n|$ for $n > 1$ and $z + \xi_0 \approx z$, we multiply Eq. (7) by $\sin(n\omega_0(1 + \Omega)t)$ and $\cos(n\omega_0(1 + \Omega)t)$, and integrate to derive the equations for \tilde{A}_n as

$$\int_0^\pi \frac{d\tau}{\pi} F_c(z + A_1 \cos \tau) \cos n\tau = \frac{1}{2} \text{Re}[\tilde{A}_n \hat{H}_n^{-1}], \quad (12)$$

$$\int_0^\pi \frac{d\tau}{\pi} \Gamma(z + A_1 \cos \tau) \sin \tau \sin n\tau = \delta_{n1} \left(\frac{kA_d}{2A_1\omega_0(1 + \Omega)} \right) - \frac{1}{2A_1\omega_0(1 + \Omega)} \text{Im}[\tilde{A}_n \hat{H}_n^{-1}]. \quad (13)$$

Here, $\hat{H}_n \equiv H[in\omega_0(1 + \Omega)] i^{1-n}$, different from \tilde{H}_n in the previous subsection. Solving Eqs. (12) and (13), we can analytically derive the multiharmonic response \tilde{A}_n up to an arbitrary order n . Note these expressions are more general than those previously reported [37], as the latter uses the low bandwidth ($Q \gg 1$) approximation.

The *exact* inversion formulas for the conservative and dissipative forces are similarly derived as the amplitude-modulation counterparts,

$$F_c(z) = \sum_{m=1}^\infty \left\{ (-1)^m (2m-1) \times \int_z^\infty \frac{dz'}{A_1} \text{Re}[\tilde{A}_{2m-1}(z') \hat{H}_{2m-1}^{-1}(z')] \right\}, \quad (14)$$

$$\Gamma(z) = \frac{kA_d(z)}{A_1\omega_0[1 + \Omega(z)]} + \sum_{m=1}^\infty \frac{(-1)^m}{m A_1\omega_0[1 + \Omega(z)]} \text{Im}[\tilde{A}_{2m-1}(z) \hat{H}_{2m-1}^{-1}(z)]. \quad (15)$$

Let us make several remarks on our theoretical derivation. First, for a conservative system ($\Gamma(z) \equiv 0$), the higher harmonic signals are given explicitly as [see Eq. (S6) in Supplemental Material [39]],

$$\tilde{A}_n = 2\hat{H}_n \sum_{k=0}^\infty \frac{A_1^{2k+n}}{2^{(2k+n)} k!(k+n)!} \frac{d^{2k+n}}{dz^{2k+n}} F_c(z), \quad (16)$$

where the leading term is proportional to the n th derivative of F_c and the rest is attenuated exponentially. Thus, the higher harmonic signals due to interatomic forces that follow the inverse power laws are more localized close to the surface atoms, which explains the enhanced resolution imaging in MHAFFM [29]. Second, the reconstruction formulas for both conservative and dissipative forces require \tilde{A}_n 's of odd n . This can be intuitively explained for the conservative part using the fact that we derive F_c by integrating the exact value of dF_c/dz . In Eq. (16), the odd (even)-order derivatives of F_c are linear combinations of the odd (even) harmonics (and vice versa), which explains why dF_c/dz , and consequently its integral F_c , is a function of odd harmonics. Third, F_c can be efficiently approximated by using a finite upper bound M in the summations in Eqs. (10) and (14), with M corresponding to the order of approximation. Then, the calculations are reduced to M integrations that each require $O(N)$ computation time, where N is the number of discrete data points. The resulting computation time of this scheme is $O(MN)$, dramatically faster than both the SJ method [14] that requires integrations for each point [$O(N^2)$], and the matrix method [9] that involves inversion of $N \times N$ matrices [$O(N^k)$ with $2.373 \leq k \leq 3$ depending on the algorithm used]. Next, while we assume a single eigenmode of the cantilever, the analogous reconstruction formulas can also be

derived assuming multiple eigenmodes where one of its resonance frequencies is an exact multiple of ω_{res} , enhancing the corresponding higher harmonic responses [42]. For this, we only need to replace $H(i\omega)$, used to define \tilde{H}_n and \hat{H}_n , respectively, in Eqs. (10)–(11) and Eqs. (14)–(15), by the transfer function of the corresponding eigenmode. Lastly, dissipative forces that cannot be expressed as a velocity-dependent form shown in Eq. (6), such as defect states in the tip or sample, are not considered in our theory. Still, conservative forces can be recovered from the given formulas even if the dissipation is not explicitly dependent on \dot{z} , but is an odd function with respect to path inversion of the tip trajectory (e.g., dependent on z^3, z^5, \dots) [37]. This is because the integration that is used to derive Eqs. (8) and (12) cancels out all odd functions, and the reconstruction formulas for conservative force are directly derived from those equations.

Results.—We verify that our reconstruction formulas are exact for the entire range of oscillation amplitudes and tip-sample separations. First, we generate multiharmonic signals \tilde{A}_n with respect to the model force for both AM-AFM and FM-AFM using Eqs. (8)–(9) and Eqs. (12)–(13), respectively. We use the Lennard-Jones (LJ)-type force for our analysis, which is defined as

$$F_{\text{LJ}}(z) = F_0 \left(\frac{l^6}{3z^6} - \frac{l^2}{z^2} \right), \quad (17)$$

where $F_0 = 0.9$ nN is a constant and $l = 0.3$ nm is the characteristic length. The LJ-type force has the inflection point $z_{\text{inf}} = 1.24l$ where the curvature of the force changes sign, force-minimum point $z_{f \text{ min}} = l$, and potential-minimum point $z_{p \text{ min}} = 0.76l$. To choose the oscillation amplitude, we invoke the inflection point test of Sader *et al.* [18], which gives the amplitude range where single frequency-based conventional force reconstruction methods are unreliable:

$$\sqrt{-\frac{F'_{\text{int}}(z_{\text{inf}})}{F'''_{\text{int}}(z_{\text{inf}})}} \leq A_1 \leq \frac{z_{\text{inf}}}{2}. \quad (18)$$

For the LJ-type force, the corresponding amplitude range is $0.22l < A_1 < 0.62l$, which is comparable to λ of the attractive force ($0.5l$). For comprehensive analysis, we use amplitudes that are small ($0.1l = 0.03$ nm), intermediate ($0.33l = 0.1$ nm), and large ($0.66l = 0.2$ nm) with respect to Eq. (18), for the free (fixed) oscillation amplitude in AM-AFM (FM-AFM) to generate the multiharmonic signals. The mechanical parameters of the cantilever and the spacing of the data points were set to values typical in ambient (vacuum) condition tuning fork-based DFM experiments with $N \approx 5000$ (see Supplemental Material SM2 [39]).

Now, we reconstruct the interaction forces from the generated AM-AFM and FM-AFM multiharmonic signals, as shown in Figs. 1 and 2, using an order M approximation of the formulas [Eqs. (10) and (14)] with varying M .

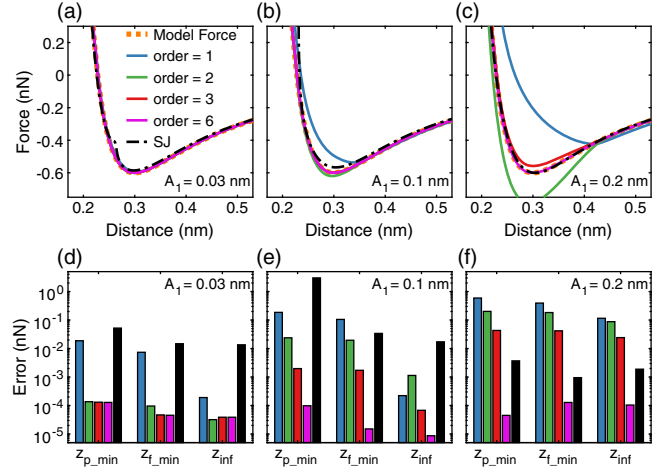


FIG. 1. Analysis of the reconstructed force in AM-AFM for different free oscillation amplitudes A_1 . (a)–(c) Reconstructed force-distance curves using different orders of approximation and those of the Sader-Jarvis method (black) are presented and compared to the model force F_{LJ} (orange). (d)–(f) Reconstruction errors are calculated for each plot at the potential minimum $z_{p \text{ min}}$, force minimum $z_{f \text{ min}}$, and inflection point z_{inf} of F_{LJ} . As shown, increasing the order of approximation reduces the overall error observed at the specific points.

Increasing M leads to more accurate reconstruction results in Figs. 1(a)–1(c) and Figs. 2(a)–2(c) as well as less errors at $z_{p \text{ min}}$, $z_{f \text{ min}}$, and z_{inf} in Figs. 1(d)–1(f) and Figs. 2(d)–2(f), demonstrating the exactness of the reconstruction formulas. Moreover, since the accuracy of the approximation is compromised by the magnitude of the higher harmonics of order $> 2M - 1$, smaller amplitudes result in more accurate reconstructions even at smaller M . For example, the reconstruction errors for AM-AFM at $z_{f \text{ min}}$ in Figs. 1(d)–1(f) are given as 0.02%, 0.3%, and 0.02% using $M = 2$ (small amplitude), 3 (intermediate amplitude), and 6 (large amplitude), respectively. For FM-AFM, the reconstruction errors at $z_{f \text{ min}}$ in Figs. 2(d)–2(f) are given as 0.03%, 0.8%, and 0.25% using the same M values for each amplitude, except for a large amplitude ($M = 9$). These results demonstrate superior accuracy over the SJ method by an order of magnitude for intermediate and large amplitudes, and by 2 orders of magnitude for smaller amplitudes. In addition, our approach displays superior computational efficiency, with at least tenfold decrease in the computation time compared to the SJ method (see Supplemental Material SM3 [39]).

Let us now discuss the robustness of the reconstruction formulas. The resolving power of DFM between two distinct interatomic force laws is dependent on how precisely the forces can be recovered. However, in FM-AFM operations, the precision of force recovery is compromised by the instability of the oscillation amplitude. Although ffeedback is used to maintain a constant amplitude, the nonconservative tip-sample interaction can lead to

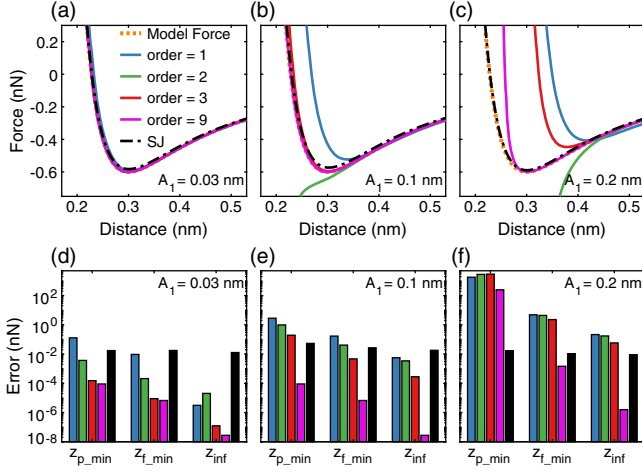


FIG. 2. Force reconstruction in FM-AFM using different fixed oscillation amplitudes A_1 . (a)–(c) Reconstructed force-distance curves of the model force F_{LJ} (orange) using different orders of approximation of the reconstruction formulas. (d)–(f) Reconstruction errors calculated at $z_{p\min}$, $z_{l\min}$, and z_{inf} . The results of the Sader-Jarvis method (black) are also shown for comparison. Similar to the results in AM-AFM, the reconstruction accuracy at such points increases when using higher orders of approximation, reflecting the exactness of the reconstruction formulas.

variations in the amplitude during the gradual approach of the cantilever, causing spurious results in force reconstruction. This is expected to be maximized in single frequency-based reconstruction procedures when the amplitude is in the intermediate range [Eq. (18)] and when the force has points not infinitely differentiable with respect to z [18], which all lead to greater anharmonic motion of the cantilever within the regime where the force changes rapidly. To verify the robustness with respect to the amplitude instability, we perform force reconstruction using the *set* oscillation amplitudes $A_{1,\text{set}}$ having $\pm 5\%$ error with respect to the *actual* oscillation amplitude $A_{1,\text{actual}}$ [18]. As the model force, we use the Stillinger-Weber (SW) type, which approximates the forces between two silicon atoms, because it changes rapidly at $z \approx 350$ pm. The multiharmonic signals are generated with $A_{1,\text{actual}} = 50$ pm, which lies in the range of Eq. (18), and the same parameters used for the LJ force. Then, we recover the forces using $A_{1,\text{set}} = 50$ pm (0% error), 52.5 pm (+5% error), 47.5 pm (−5% error), as shown in Figs. 3(a) and 3(b). The minimum force from the SJ method shows a significant error (8.4%, solid line) and the greatest variance ($\pm 5.0\%$, dotted lines), whereas they are reduced significantly to 0.2% and $\pm 1.0\%$, respectively, in the reconstruction using $M = 3$. We also find accuracy improvement corresponding to 7.1% of the absolute value of the Derjaguin-Muller-Toporov (DMT)–type force, indicating that our method can be used for accurate measurements of a wide range of forces (see Supplemental Material SM3 [39]). Furthermore, we perform the same reconstruction procedures using the model force rescaled by different

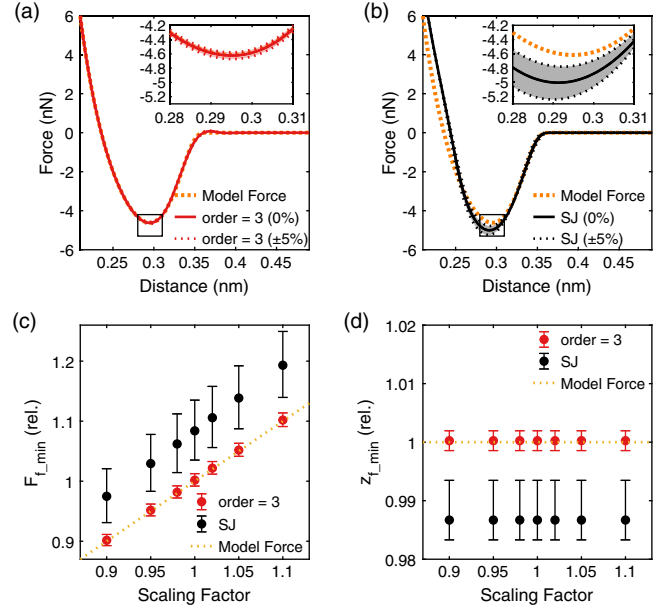


FIG. 3. Robustness of force reconstruction with respect to amplitude error. (a)–(b) Reconstructed forces from the signals generated using the SW-type force (orange) and fixed oscillation amplitude $A_{1,\text{actual}} = 50$ pm, assuming no error (0% error, solid line) and $\pm 5\%$ error (dotted line) with respect to $A_{1,\text{actual}}$. Different scaling factors are used to rescale the SW-type force, where the force minimum of the reconstruction results are evaluated in terms of (c) relative force and (d) relative distance with respect to the original SW type force minimum. The error bars delimit the relative position of the force minimum assuming $\pm 5\%$ amplitude error.

scaling factors; we use 0.9, 0.95, 0.98, 1, 1.02, 1.05, and 1.1, to observe the resolving power of the formulas. Quantitative analysis of the force minimum of the reconstruction results in Figs. 3(c) and 3(d) reveals that multiharmonic consideration allows us to resolve the rescaled SW-type forces at $\approx 2\%$ precision, which is a fivefold improvement over the SJ method.

Conclusion.—We have developed a universal theory of DFM based on multiharmonic signal analysis. Our method enables exact and robust reconstruction of the conservative and dissipative forces in both amplitude- and frequency-modulation AFM, regardless of the oscillation amplitudes and tip-sample distances. Even when approximated reconstruction formulas are used, higher accuracy over the SJ method with less computation time can be obtained. Force reconstruction using the multiharmonic signal analysis has also been demonstrated to be robust with respect to the oscillation amplitude error, overcoming the intrinsic reconstruction instability of the conventional methods. Our theoretical platform provides versatility and efficiency for accurate and precise force measurements beyond the limits of conventional DFM.

This work was supported by the National Research Foundation of Korea (NRF) grant funded by the Korea government (MSIP) (No. 2016R1A3B1908660).

*Corresponding author.

whjhe@snu.ac.kr

- [1] G. Binnig, C.F. Quate, and C. Gerber, Atomic Force Microscope, *Phys. Rev. Lett.* **56**, 930 (1986).
- [2] F.J. Giessibl, Atomic-resolution of the silicon (111)-(7 × 7) surface by atomic-force microscopy, *Science* **267**, 68 (1995).
- [3] B. Cappella and G. Dietler, Force-distance curves by atomic force microscopy, *Surf. Sci. Rep.* **34**, 1 (1999).
- [4] R. Garcia and R. Prez, Dynamic atomic force microscopy methods, *Surf. Sci. Rep.* **47**, 197 (2002).
- [5] R. Garcia, *Amplitude Modulation Atomic Force Microscopy* (WileyVCH, Singapore, 2010).
- [6] F.J. Giessibl, Advances in atomic force microscopy, *Rev. Mod. Phys.* **75**, 949 (2003).
- [7] U. Dürig, Extracting interaction forces and complementary observables in dynamic probe microscopy, *Appl. Phys. Lett.* **76**, 1203 (2000).
- [8] B. Gotsmann, B. Anczykowski, C. Seidel, and H. Fuchs, Determination of tip-sample interaction forces from measured dynamic force spectroscopy curves, *Appl. Surf. Sci.* **140**, 314 (1999).
- [9] F.J. Giessibl, A direct method to calculate tip-sample forces from frequency shifts in frequency-modulation atomic force microscopy, *Appl. Phys. Lett.* **78**, 123 (2001).
- [10] M. Lee and W. Jhe, General Theory of Amplitude-Modulation Atomic Force Microscopy, *Phys. Rev. Lett.* **97**, 036104 (2006).
- [11] S. Hu and A. Raman, Inverting amplitude and phase to reconstruct tip-sample interaction forces in tapping mode atomic force microscopy, *Nanotechnology* **19**, 375704 (2008).
- [12] O.E. Dagdeviren, C. Zhou, E.I. Altman, and U.D. Schwarz, Quantifying tip-sample interactions in vacuum using cantilever-based sensors: An analysis, *Phys. Rev. Applied* **9**, 044040 (2018).
- [13] J. Welker, E. Illek, and F.J. Giessibl, Analysis of force-deconvolution methods in frequency-modulation atomic force microscopy, *Beilstein J. Nanotechnol.* **3**, 238 (2012).
- [14] J.E. Sader and S.P. Jarvis, Accurate formulas for interaction force and energy in frequency modulation force spectroscopy, *Appl. Phys. Lett.* **84**, 1801 (2004).
- [15] A.F. Payam, D. Martin-Jimenez, and R. Garcia, Force reconstruction from tapping mode force microscopy experiments, *Nanotechnology* **26**, 185706 (2015).
- [16] A.J. Katan, M.H. van Es, and T.H. Oosterkamp, Quantitative force versus distance measurements in amplitude modulation afm: a novel force inversion technique, *Nanotechnology* **20**, 165703 (2009).
- [17] O.E. Dagdeviren and U.D. Schwarz, Accuracy of tip-sample interaction measurements using dynamic atomic force microscopy techniques: Dependence on oscillation amplitude, interaction strength, and tip-sample distance, *Rev. Sci. Instrum.* **90**, 033707 (2019).
- [18] J.E. Sader, B.D. Hughes, F. Huber, and F.J. Giessibl, Interatomic force laws that evade dynamic measurement, *Nat. Nanotechnol.* **13**, 1088 (2018).
- [19] F. Huber and F.J. Giessibl, Experimental use of the inflection point test for force deconvolution in frequency-modulation atomic force microscopy to turn an ill-posed situation into a well-posed one by proper choice of amplitude, *J. Appl. Phys.* **127**, 184301 (2020).
- [20] F.J. Giessibl, H. Bielefeldt, S. Hembacher, and J. Mannhart, Calculation of the optimal imaging parameters for frequency modulation atomic force microscopy, *Appl. Surf. Sci.* **140**, 352 (1999).
- [21] L. Gross, F. Mohn, N. Moll, P. Liljeroth, and G. Meyer, The chemical structure of a molecule resolved by atomic force microscopy, *Science* **325**, 1110 (2009).
- [22] F. Pielmeier and F.J. Giessibl, Spin Resolution and Evidence for Superexchange on NiO(001) Observed by Force Microscopy, *Phys. Rev. Lett.* **110**, 266101 (2013).
- [23] N. Pavliček and L. Gross, Generation, manipulation and characterization of molecules by atomic force microscopy, *Nat. Rev. Chem.* **1**, 0005 (2017).
- [24] F. Huber, J. Berwanger, S. Polesya, S. Mankovsky, H. Ebert, and F.J. Giessibl, Chemical bond formation showing a transition from physisorption to chemisorption, *Science* **366**, 235 (2019).
- [25] J. Berwanger, S. Polesya, S. Mankovsky, H. Ebert, and F.J. Giessibl, Atomically Resolved Chemical Reactivity of Small Fe Clusters, *Phys. Rev. Lett.* **124**, 096001 (2020).
- [26] S. Crittenden, A. Raman, and R. Reifengerger, Probing attractive forces at the nanoscale using higher-harmonic dynamic force microscopy, *Phys. Rev. B* **72**, 235422 (2005).
- [27] R.W. Stark and W.M. Heckl, Higher harmonics imaging in tapping-mode atomic-force microscopy, *Rev. Sci. Instrum.* **74**, 5111 (2003).
- [28] F.J. Giessibl, Higher-harmonic atomic force microscopy, *Surf. Interface Anal.* **38**, 1696 (2006).
- [29] S. Hembacher, F.J. Giessibl, and J. Mannhart, Force microscopy with light-atom probes, *Science* **305**, 380 (2004).
- [30] F. Gramazio, M. Lorenzoni, F. Perez-Murano, E. R. Trinidad, U. Staufer, and J. Fraxedas, Functional dependence of resonant harmonics on nanomechanical parameters in dynamic mode atomic force microscopy, *Beilstein J. Nanotechnol.* **8**, 883 (2017).
- [31] F. Gramazio, M. Lorenzoni, F. Perez-Murano, L. Evangelio, and J. Fraxedas, Quantification of nanomechanical properties of surfaces by higher harmonic monitoring in amplitude modulated afm imaging, *Ultramicroscopy* **187**, 20 (2018).
- [32] N.H. Shaik, R.G. Reifengerger, and A. Raman, Nanomechanical mapping in air or vacuum using multi-harmonic signals in tapping mode atomic force microscopy, *Nanotechnology* **31**, 455502 (2020).
- [33] A. Raman, S. Trigueros, A. Cartagena, A. P. Stevenson, M. Susilo, E. Nauman, and S.A. Contera, Mapping nanomechanical properties of live cells using multi-harmonic atomic force microscopy, *Nat. Nanotechnol.* **6**, 809 (2011).
- [34] D.B. Haviland, Quantitative force microscopy from a dynamic point of view, *Curr. Opin. Colloid Interface Sci.* **27**, 74 (2017).
- [35] C. Hutter, D. Platz, E.A. Tholen, T.H. Hansson, and D.B. Haviland, Reconstructing Nonlinearities with Intermodulation Spectroscopy, *Phys. Rev. Lett.* **104**, 050801 (2010).
- [36] S. Kawai, S. Hafizovic, T. Glatzel, A. Baratoff, and E. Meyer, Rapid reconstruction of a strong nonlinear property by a multiple lock-in technique, *Phys. Rev. B* **85**, 165426 (2012).

- [37] U. Dürig, Interaction sensing in dynamic force microscopy, *New J. Phys.* **2**, 5 (2000).
- [38] B. Anczykowski, B. Gotsmann, H. Fuchs, J. P. Cleveland, and V. B. Elings, How to measure energy dissipation in dynamic mode atomic force microscopy, *Appl. Surf. Sci.* **140**, 376 (1999).
- [39] See Supplemental Material at <http://link.aps.org/supplemental/10.1103/PhysRevLett.126.076804> for detailed information on the derivation of our force reconstruction formulas, the generation of multiharmonic signals using the Lennard-Jones type force, the force reconstruction results using multiharmonic signals, and the reconstruction robustness with respect to measurement noise, which includes Refs. [40,41].
- [40] F. J. Giessibl, F. Pielmeier, T. Eguchi, T. An, and Y. Hasegawa, Comparison of force sensors for atomic force microscopy based on quartz tuning forks and length-extensional resonators, *Phys. Rev. B* **84**, 125409 (2011).
- [41] J. Kim, B. Sung, B. I. Kim, and W. Jhe, Optimization of force sensitivity in q -controlled amplitude-modulation atomic force microscopy, *J. Appl. Phys.* **114**, 054302 (2013).
- [42] O. Sahin, C. F. Quate, O. Solgaard, and A. Atalar, Resonant harmonic response in tapping-mode atomic force microscopy, *Phys. Rev. B* **69**, 165416 (2004).